Nanoscale

COMMUNICATION

View Article Online
View Journal | View Issue

Published on 12 February 2018. Downloaded by University of Wisconsin - Madison on 21/03/2018 19:01:49.

Check for updates

Cite this: *Nanoscale*, 2018, **10**, 5054

Received 5th December 2017,
Accepted 11th February 2018

DOI: 10.1039/c7nr09042k

rsc.li/nanoscale

A wafer-scale 1 nm $Ni(OH)_2$ nanosheet with superior electrocatalytic activity for the oxygen evolution reaction†

Peng Tian,[a,b] Yanhao Yu,[a] Xin Yin[a] and Xudong Wang *[a]

A wafer-scale 1.4 nm ultrathin $Ni(OH)_2$ nanosheet was synthesized by ionic layer epitaxy. This free-standing $Ni(OH)_2$ nanosheet was directly used to catalyze the oxygen evolution reaction (OER). At a current density of 10 mA cm^{-2}, the overpotential reached 295 mV (*vs.* RHE) in Fe-rich 1 M NaOH. This 1.4 nm $Ni(OH)_2$ nanosheet showed a very high turnover frequency of 5.47 s^{-1} and a mass activity of more than 2×10^4 A g^{-1} at an overpotential of 300 mV. Such a high electrocatalytic mass activity of the $Ni(OH)_2$ nanosheet was more than 2 orders of magnitude higher than those of typical OER catalysts. The capability of producing wafer-scale nanometer-thick nanosheets offers a promising strategy to improve the mass efficiency of electrochemical catalysts, which is particularly valuable for preserving rare and precious catalyst materials.

Electrochemical water splitting is a promising strategy for converting electrical energy into chemical fuel.[1,2] In a water-splitting system, electrochemical catalysts are normally used to facilitate the hydrogen evolution reaction (HER) and oxygen evolution reaction (OER) on the cathode and anode, respectively.[3,4] Many transition-metal compounds, such as borides, nitrides, oxides, hydroxides, phosphides, sulfides, and selenides have been explored as promising candidates for OER catalysts.[5–11] Among them, Ni-based oxides/hydroxides appeared to be one of the most competitive materials which give a low overpotential and high current density due to the active species of $Ni^{III/IV}$ for OER catalysts.[12–22] Very recently, two dimensional (2D) nanomaterials, owing to their abundant active sites, delocalized spin states and high electrical conductivity, showed great promise for further promoting the electrochemical catalytic activity.[23–29] For example, metallic nanosheets of 1T-MoS_2 grown on graphite showed a dramatically enhanced HER catalytic behavior.[23] 2D nanostructured WSe_2 manifested much higher performance for electrocatalytic CO_2 reduction compared to bulk transition metal dichaldogenides.[24] Although significantly enhanced catalytic performance was demonstrated in comparison with their bulk form, these materials intrinsically are not the optimal catalytic material selection. The best solution is to create 2D nanostructures from the catalytic material to raise the existing good catalytic performance to a new level. The record high catalytic performance from nanometer-thicker Co–Co_3O_4 is a good example of this strategy.[25] However, since these materials typically do not have a layered crystal structure, they could only be made with sizes usually smaller than 1 μm. This remains a great challenge for system-level development where wafer-scale uniform thickness distribution is required. To address this challenge, here we report the development of a 1.4 nm $Ni(OH)_2$ nanosheet OER catalyst on the wafer scale by ionic layer epitaxy (ILE). The uniform nanometer thickness of the $Ni(OH)_2$ nanosheet across the entire wafer surface offered orders of magnitude higher mass electrochemical activity compared to typical OER catalysts. This development marks a new cornerstone for the development of an efficient electrochemical catalyst.

The $Ni(OH)_2$ nanosheet was synthesized using nickel nitrate hexahydrate and hexamethylenetetramine (HMT) as precursors, and templated with a monolayer of oleic acid surfactant at the water surface (see the ESI† for the synthesis details). Due to the very low precursor concentration, growth only occurred at the polarized interface where the Ni^{2+} ions were concentrated within the electrical double layer. The growth mechanism is detailed in previous publications.[30–32] In this work, the interaction between the oleic acid and precursors could be briefly described as follows. At 60 °C, HMT decomposed into HCHO and ammonium hydroxide, forming an alkaline environment. Under alkaline conditions, oleic acid will dissociate into negatively charged oleate. The positively charged Ni^{2+} ions were concentrated under the monolayer of oleate, forming a Stern layer of Ni^{2+} ions. Then, the Ni^{2+} ions in the Stern layer could reach supersaturation and crystallize into a layer of $Ni(OH)_2$. The critical nucleation size of $Ni(OH)_2$

[a]*Department of Material Sciences and Engineering, University of Wisconsin-Madison, Madison, WI 53706, USA. E-mail: xudong.wang@wisc.edu*
[b]*School of Chemical Engineering, Dalian University of Technology, Dalian, 116023, China*

†Electronic supplementary information (ESI) available. See DOI: 10.1039/c7nr09042k

This journal is © The Royal Society of Chemistry 2018

Published on 12 February 2018. Downloaded by University of Wisconsin - Madison on 21/03/2018 19:01:49.

could be limited by the carboxylic groups bonding to $Ni(OH)_2$ crystals. Due to the complete coverage of the surfactant monolayer, the $Ni(OH)_2$ nanosheet could be grown as large as the entire solution surface in the reactor. In order to transfer the entire nanosheet, a 3-inch Si wafer was placed at the bottom of the solution prior to the growth (Fig. 1a). By slowly removing the nutrient solution after the growth, the nanosheet was completely transferred to the Si wafer surface (Fig. 1b). After drying, the Si wafer still exhibited a very clear and smooth surface without any observable additives or non-uniform optical diffractions (Fig. 1c), confirming the extremely high wafer-scale uniformity. Fig. 1d is a typical SEM image of an as-transferred nanosheet on a Si substrate. No visible contrast variation could be observed because the nanosheet was continuous and uniform in thickness. The same featureless images were obtained for the entire substrate, revealing the extreme uniformity of the nanosheet geometry and coverage (Fig. S1†). A few small cracks could be found as shown in Fig. 1e, which was used to confirm the existence of the nanosheet. The atomic force microscopy (AFM) topography image revealed that the nanosheet surface was extremely smooth and flat (Fig. 1f). Sporadic particles observed on the nanosheet surface may be the contaminants picked up from the reaction solution during the transfer process. Two line profiles along the crack area were extracted and are shown in Fig. 1g, which confirmed that the thickness of the nanosheet was 1.4 nm and uniform across the entire nanosheet.

X-ray photoelectron spectroscopy (XPS) was employed to probe the elemental information and bonding states of the nanosheet. The full XPS survey spectra clearly showed the Ni, O, C and Si peaks detected from the as-transferred nanosheet on a Si substrate (Fig. 2a). To further reveal the chemical state of the Ni atom, the Ni 2p XPS peak of the nanosheet was individually scanned and deconvoluted (Fig. 2b). The peak at 855.5 eV can be attributed to Ni^{2+} in $Ni(OH)_2$, evidencing that the bulk component of this nanosheet was $Ni(OH)_2$.

Transmission electron microscopy (TEM) was then used to characterize the crystal structure of the $Ni(OH)_2$ nanosheets. Fig. 2c shows an as-synthesized nanosheet on a holey carbon TEM grid. Due to the extreme flexibility, wrinkles or overlaps could often be observed on the suspended regions. The high-resolution TEM (HRTEM) image revealed the polycrystalline feature of the $Ni(OH)_2$ nanosheet, where the individual domain was found to be ~5 nm (Fig. 2d). From the image, the (101) *d*-spacing was found to be 0.235 nm. The corresponding selective area electron diffraction (SAED) pattern exhibited a semi-continuous ring pattern (inset of Fig. 2c), in which the diffraction rings can be indexed to the (100), (101), (102) and (110) atomic planes of trigonal β-$Ni(OH)_2$ (space groups $P\bar{3}m1$, a = 0.312 nm, c = 0.46 nm, α = 90°, β = 90°, and γ = 120°).

To study the catalytic behavior associated with the ultra-small thickness towards the OER, the $Ni(OH)_2$ nanosheet was transferred onto a FTO glass (Fig. S2†). As a comparison, the OER activities of thicker $Ni(OH)_2$ layers, commercial RuO_2 and bare FTO glass were evaluated using the same configuration. The thicker $Ni(OH)_2$ layers were prepared by either ILE or

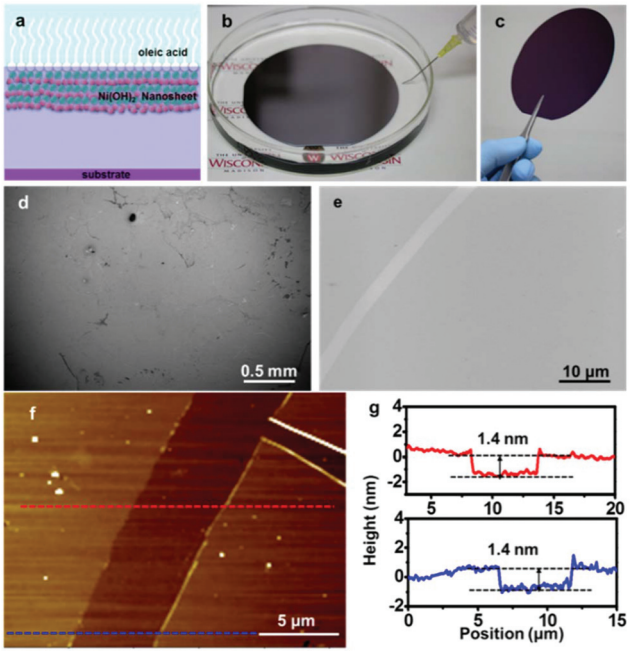

Fig. 1 Growth and morphology of $Ni(OH)_2$ nanosheets. (a) Schematic diagram of a growing $Ni(OH)_2$ nanosheet in a culture dish. (b) Optical image of depositing an $Ni(OH)_2$ nanosheet on a Si wafer. (c) Optical image of a Si wafer uniformly covered with a $Ni(OH)_2$ nanosheet. (d) and (e) SEM images of a $Ni(OH)_2$ nanosheet on the Si substrate surface. (f) AFM topography scan of a cracking area from the $Ni(OH)_2$ nanosheet. (g) The height profiles along the blue and red lines in (f) showing a very uniform film thickness of 1.4 nm.

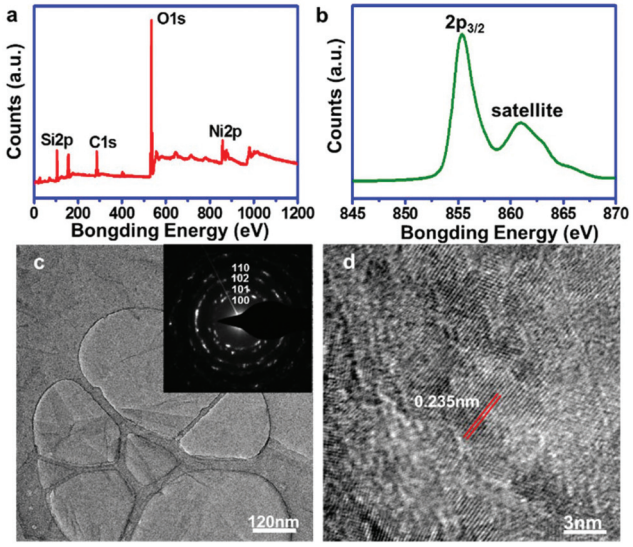

Fig. 2 Structural characterization. (a) XPS spectra of the $Ni(OH)_2$ nanosheet on an Si substrate. (b) High-revolution XPS of the Ni^{2+} peak. (c) A low-magnification TEM image of a $Ni(OH)_2$ nanosheet supported on a holey carbon TEM grid. The inset is the corresponding SAED pattern of the $Ni(OH)_2$ nanosheet and (d) HRTEM image of the $Ni(OH)_2$ nanosheet showing its polycrystalline nature.

Published on 12 February 2018. Downloaded by University of Wisconsin - Madison on 21/03/2018 19:01:49.

electrodeposition (see the Experimental section in the ESI and Fig. S3 and S4†) and their thicknesses were found to be 7.0 nm and 230 nm for these methods. The commercial RuO_2 was deposited on FTO by the solvent evaporation method (see the detailed information in the ESI and Fig. S5†). Fig. 3a illustrates the current density–overpotential (j–η) curves of the 1.4 nm Ni$(OH)_2$ nanosheet measured in 1 M NaOH solution in comparison with the other two thicker Ni$(OH)_2$ films, commercial RuO_2 and bare FTO. All of the Ni$(OH)_2$ samples can produce a geometric current density of 10 mA cm^{-2} at η = ~330 mV, which agreed well with other reported NiO_x OER catalysts.[7,12,17] The j values of Ni$(OH)_2$ samples were larger than that of commercial RuO_2, and far higher than that of bare FTO. Moreover, it can be observed that all Ni$(OH)_2$ samples displayed an oxidation peak at η from 100 mV to 200 mV (the peaks from the 1.4 nm and 7.0 nm Ni$(OH)_2$ samples were enlarged and are shown in Fig. 3b). This oxidation feature is related to the oxidation of Ni$(OH)_2$ to NiOOH,[12,20] and is reflective of the amount of active Ni sites. The large difference of the peak areas suggested that Ni atoms inside the bulk film were also electrochemically active. Du's study showed that high oxidation state $Ni^{III/IV}$ can serve as an active species for OER catalysts.[15]

From the oxidation peak in our work, it can be seen that the thicker Ni$(OH)_2$ samples have more $Ni^{III/IV}$ sites. But their OER performance is similar to that of 1.4 nm Ni$(OH)_2$ samples. Therefore, this result indicates that not all high oxidation states of Ni sites can catalyze the OER. To estimate the exposure of active sites, the electrochemical active surface area (ECSA) and the roughness factor (RF) were calculated by CV measurements at different voltage rates (see calculations in the ESI, Fig. S6 and Table S3†). The ECSA values in this work are smaller than those from other studies reported due to the low ECSA and RF of FTO glass.[18] The ECSA values of the electrodes that covered 1.4 nm, 7.0 nm and 230 nm Ni$(OH)_2$ layers are 0.037 cm^2, 0.035 cm^2, and 0.027 cm^2, respectively, indicating that the number of active sites is similar in different thickness Ni$(OH)_2$. Moreover, it can be observed that the ECSA and RF values of commercial RuO_2 were much higher than those of the Ni$(OH)_2$ samples (Fig. S6 and Table S3†). However, RuO_2 showed much lower OER performance compared to Ni$(OH)_2$. This result could be attributed to the good conductivity, but poor intrinsic OER catalytic activity of RuO_2.

Electrochemical impedance spectroscopy (EIS) was used to characterize the surface kinetics of the Ni$(OH)_2$ films, commercial RuO_2 and bare FTO. The Nyquist plots are shown in Fig. 3c and Fig. S7a and b.† An $R_u(R_{ct}C)$ equivalent circuit was used to fit the EIS parameters (as shown in Fig. S7c†), where R_u is the series resistance that includes the internal resistance of the electrode, R_{ct} is the charge transfer resistance, and C is the capacitance. The data are summarized in Table S4.† All the Ni$(OH)_2$ samples showed a very close R_{ct}, suggesting that there was no visible variation of the charge transfer resistance across the solid/electrolyte interface in these Ni$(OH)_2$-FTO electrodes. And it can be seen that the R_{ct} values of bare FTO (15 052 Ω) and RuO_2 (380 Ω) are far higher than that of Ni$(OH)_2$ (about 70 Ω), which is consistent with the electrocatalytic measurements. By extrapolating the linear region of η *versus* log$j$ (Fig. 3d and Fig. S8†), the Tafel slope values of the 1.4 nm, 7.0 nm, and 230 nm Ni$(OH)_2$ films, commercial RuO_2, and bare FTO, were determined to be 41, 55, 80, 90, and 140 mV per decade, respectively. The significantly lower Tafel slope of 1.4 nm Ni$(OH)_2$ was an indication of the largely promoted interfacial kinetics as the film thickness was reduced to the nanometer scale. The ultra-thin thickness ensured that all the charge separation in the film would occur in the space charge region with only ~1 nanometer diffusion length.

The mass activity of an electrocatalyst is particularly meaningful in commercial applications. As shown in Fig. 3e, a remarkable mass activity of 4662 A g^{-1} was obtained from the 1.4 nm Ni$(OH)_2$ nanosheet at η = 300 mV, approximately 3.6, 120 and 650 times higher than that of the 7.0 nm Ni$(OH)_2$ layers, 230 nm Ni$(OH)_2$ layers, and commercial RuO_2, respectively. The intrinsic activity also plays a crucial role in optimizing the overall OER activity, which could be estimated by the turnover frequency (TOF). The TOF values are defined as the number of O_2 molecules evolved per electrochemically accessible Ni (or Ru) site per second. The TOF values were calculated by:

$$\mathrm{TOF} = \frac{j \times A}{4 \times F \times m}$$

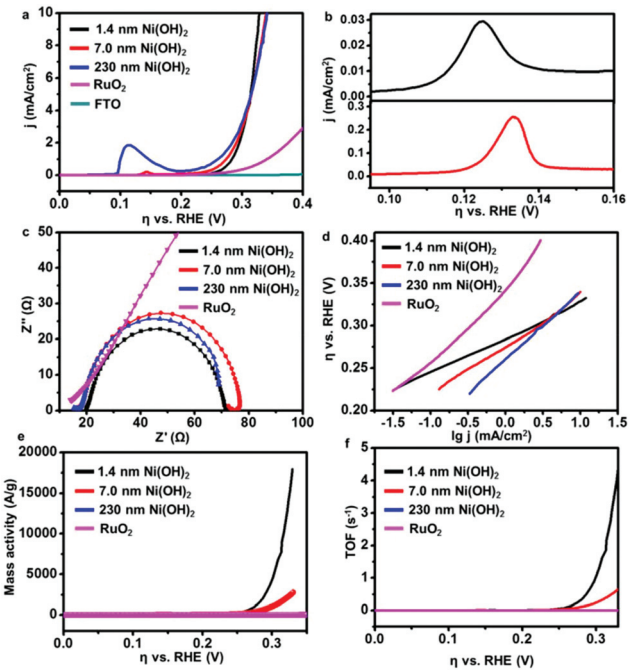

Fig. 3 Electrocatalytic performance comparison of the 1.4 nm Ni$(OH)_2$ nanosheet (black), 7.0 nm Ni$(OH)_2$ layers (red), 230 nm (blue) Ni$(OH)_2$ layers, commercial RuO_2 (pink) and bare FTO (green). (a) The j–η curves measured in 1 M NaOH aqueous solution for OER. (b) Oxidation peaks of 1.4 nm (top) and 7.0 nm (bottom) Ni$(OH)_2$. (c) Nyquist plots measured in 1 M NaOH solution at a potential of 620 mV *vs.* Hg/HgO. (d) Tafel plots extrapolated from the linear region of η *versus* log j (e) Mass activity and (f) TOF determined from j as a function of η.

 This journal is © The Royal Society of Chemistry 2018

Published on 12 February 2018. Downloaded by University of Wisconsin - Madison on 21/03/2018 19:01:49.

where A is the surface area of the electrode, F is the Faraday constant, and m is the number of moles of the catalyst. The m of $Ni(OH)_2$ could be calculated from the effective thickness (ESI, Table S1†) and molecular weight of $Ni(OH)_2$. As shown in Fig. 3f, when a η of 300 mV is applied, a TOF of 1.12 s^{-1} is recorded for the 1.4 nm $Ni(OH)_2$ catalyst, that is about 3.6-, 120- and 450-times higher than that of the 7.0 nm and 230 nm $Ni(OH)_2$ layers and commercial RuO_2, respectively, further confirming the outstanding intrinsic activity of the ultrathin $Ni(OH)_2$ in OER catalysis. The significant enhancement in the electrocatalytic activity could be attributed to the largely facilitated electron transfer from the ultra-thin nanosheet to the substrate.

Moreover, the very recent work showed that an Fe-rich electrolyte could largely improve the OER activity of NiO_x, which depends on the role of Fe in the local structure, rather than in the bulk or on the average electrochemical properties of NiO_x.[22] Herein, we measured the j–η curve and Tafel slope in the Fe-rich NaOH electrolyte, and observed obviously enhanced catalytic activity (Fig. S9†). The mass activity and TOF values of 1.4 nm $Ni(OH)_2$ in the rich-Fe NaOH electrolyte further reached up to 2.0×10^4 A g^{-1} and 5.47 s^{-1} at η = 300 mV.

To evaluate the OER performance of the 1.4 nm $Ni(OH)_2$ nanosheet, the measured data were compared to other reported OER catalysts. The values of η, mass activity and TOF are summarized in Table 1. It can be clearly seen that the 1.4 nm $Ni(OH)_2$ nanosheet exhibited similar or slightly higher values in terms of η as compared to typical electrocatalysts, including NiO_x, IrO_x, Ni–Fe oxide/LDH, and Co-based OER catalysts. And the overpotential we reported is still lower than that of other OER electrocatalysts reported recently (as shown in Table S5†). In particular, the TOF and mass activity of the $Ni(OH)_2$ nanosheet were significantly higher than other reported values.[1,7,12,17,19,33–38] Compared to the fastest NiO_x OER catalyst reported so far (TOF = 0.4–0.6 s^{-1} at η = 300 mV in an Fe-rich electrolyte),[37] the TOF of our 1.4 nm $Ni(OH)_2$ is ~10 times higher. Our very large TOF value was also two orders of magnitude higher than a typical OER catalyst such as Fe–Ni LDH.[36]

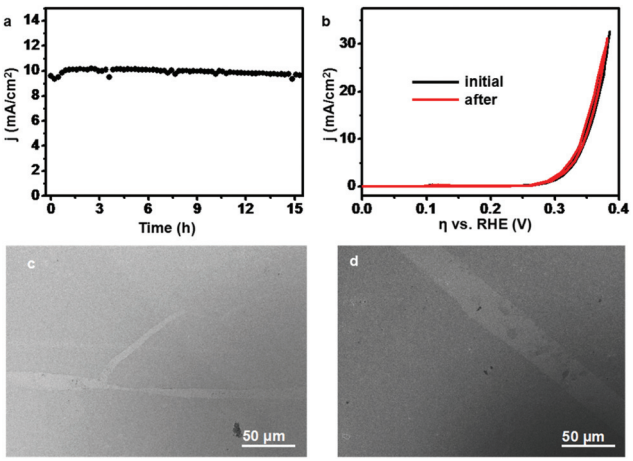

Fig. 4 Electrochemical stability evaluation. (a) Current density measured at η = 335 mV (*vs.* RHE) as a function of time. (b) j–η curves of the 1.4 nm $Ni(OH)_2$ nanosheet before (black) and after (red) 15-hour OER. (c, d) SEM images of the 1.4 nm $Ni(OH)_2$ nanosheet before (c) and after (d) the 15-hour OER operation.

Another important criterion for an OER catalyst is its operational stability. The stability of the 1.4 nm $Ni(OH)_2$ nanosheet was assessed in 1 M NaOH by recording the current density as a function of time at η = 335 mV. As shown in Fig. 4a, the j value of the $Ni(OH)_2$ nanosheet exhibited no tendency of reduction after 15 hours of continuous oxygen evolution reaction. The j–η curve also showed a very small declination (Fig. 4b, red curve) compared with the initial one (Fig. 4b, black curve). Comparing the SEM images of the $Ni(OH)_2$ nanosheets before and after the long-term operation (Fig. 4c and d), no holes or any other types of damage could be found. The nanosheet exhibited excellent integrity even around the cracked areas (Fig. S10†) where the numbers of defects and active sites are usually high. Such a good electrochemical stability could be attributed to the overall short out-plane charge diffusion length enabled by the ultrathin 2D structure with uniform thickness. This could drastically improve the charge distribution uniformity and avoid the formation of hot

Table 1 OER performance comparison between this work and others

Sample	η^a (mV)	Mass activity^b (A g^{-1})	TOF^b (s^{-1})	Ref.
$Ni(OH)_2$ nanosheet	324 ± 4 (294^c)	5058 ± 562 (23322^c)	1.22 ± 0.13 (5.47^c)	This work
2–3 nm NiO_x layer	334 ± 6	951 ± 106	0.244 ± 0.04	7
NiO nanoparticle	335 ± 5	40.7 ± 8	0.001 ± 0.0002	12 and 17
ALD NiO_x film^c	~330	896 ± 206	0.17 ± 0.04	37
2–3 nm IrO_x layer	350	—	0.046	7
2–3 nm $Ni_{0.9}Fe_{0.1}O_x$	—	—	0.4–0.6	7
NiFe LDH	430	15 ± 8.7	0.0089 ± 0.005	36
NiFe LDH/CNT	~330	1065 ± 129	0.21 ± 0.03	19
NF@NC-$CoFe_2O_4$	300	—	0.05	35
BSCF	~250	—	0.56	1 and 7
Monolayer Co	240	—	0.0915	33
FeOOH/Co/FeOOH	—	—	~0.6	34
$Ni_{0.81}Fe_{0.19}O$	310	—	<0.48	38

^{a} @ 10 mA cm^{-1}. ^{b} @ η = 300 mV. ^{c} In Fe-rich 1 M NaOH.

Published on 12 February 2018. Downloaded by University of Wisconsin - Madison on 21/03/2018 19:01:49.

spots, and thus minimize local damage to the $Ni(OH)_2$ nanosheets. Similarly, the 1.4 nm $Ni(OH)_2$ nanosheet also showed good stability under continuous reaction in an Fe-rich electrolyte, as shown in Fig S11.†

Conclusions

To conclude, we reported a wafer-scale 1.4 nm $Ni(OH)_2$ nanosheet fabricated by ILE. The $Ni(OH)_2$ nanosheet achieved significantly higher OER catalytic performance compared to thicker $Ni(OH)_2$ layers owing to the very large surface atom ratio and ultra-small cross-plane charge diffusion length. At η = 300 mV, the 1.4 nm $Ni(OH)_2$ nanosheet delivered a TOF value of 1.12 s^{-1}, which was over 3.6, 120 and 450 times higher than those of the 7.0 nm $Ni(OH)_2$ layers, 230 nm $Ni(OH)_2$ layers, and commercial RuO_2, respectively. By adding Fe salt into the electrolyte, the TOF further reached up to 5.47 s^{-1} at η = 300 mV, which was ~2 orders of magnitude higher than those of typical OER catalysts. Due to the uniform thickness across the entire wafer area, the $Ni(OH)_2$ nanosheet also exhibited excellent operational stability. This is the first report of a wafer-scale ultrathin $Ni(OH)_2$ nanosheet, which exhibited drastically enhanced electrochemical catalytic activity. This work offers a promising new catalyst solution for water splitting. The ILE technology for synthesizing wafer-scale oxide 2D nanomaterials is exceptionally valuable for developing catalysts with unprecedented mass activity from rare and precious catalyst materials.

Conflicts of interest

There are no conflicts to declare.

Acknowledgements

This work is supported by Army Research Office (ARO) under grant W911NF-16-1-0198 and the National Science Foundation through the University of Wisconsin Materials Research Science and Engineering Center (DMR-1121288).

Notes and references

1 J. Suntivich, K. J. May, H. A. Gasteiger, J. B. Goodenough and Y. S. Horn, *Science*, 2011, **334**, 1383.
2 D. Kang, T. W. Kim, S. R. Kubota, A. C. Cardiel, H. G. Cha and K. S. Choi, *Chem. Rev.*, 2015, **115**, 12839.
3 J. H. Montoya, L. C. Seitz, P. Chakthranont, A. Vojvodic, T. F. Jaramillo and J. K. Norskov, *Nat. Mater.*, 2017, **16**, 70.
4 N. T. Suen, S. F. Hung, Q. Quan, N. Zhang, Y. J. Xu and H. M. Chen, *Chem. Soc. Rev.*, 2017, **46**, 337.
5 C. Xie, Y. Y. Wang, D. F. Yan, L. Tao and S. Y. Wang, *Nanoscale*, 2017, **9**, 16059.
6 K. J. Lee, D. Y. Shin, A. Byeon, A. Lim, Y. S. Jo, A. Begley, D. H. Lim, Y. E. Sung, H. S. Park, K. H. Chae, S. W. Nam, K. Y. Lee and J. Y. Kim, *Nanoscale*, 2017, **9**, 15846.
7 L. Trotochaud, J. K. Ranney, K. N. Williams and S. W. Boettcher, *J. Am. Chem. Soc.*, 2012, **134**, 17253.
8 C. C. L. McCrory, S. Jung, I. M. Ferrer, S. M. Chatman, J. C. Peters and T. F. Jaramillo, *J. Am. Chem. Soc.*, 2015, **137**, 4347.
9 Y. Wang, T. Williams, T. Gengenbach, B. Kong, D. Y. Zhao, H. T. Wang and C. Selomulya, *Nanoscale*, 2017, **9**, 17349.
10 J. Kim, H. Jin, A. Oh, H. Baik, S. H. Jood and K. Lee, *Nanoscale*, 2017, **9**, 15397.
11 A. T. Swesi, J. Masud and M. Nath, *Energy Environ. Sci.*, 2016, **9**, 1771.
12 K. Fominykh, J. M. Feckl, J. Sicklinger, M. Doblinger, S. Bocklein, J. Ziegler, L. Peter, J. Rathousky, E. W. Scheidt, T. Bein and D. Fattakhova-Rohlfing, *Adv. Funct. Mater.*, 2014, **24**, 3123.
13 O. D. Morales, D. F. Suspedra and M. T. M. Koper, *Chem. Sci.*, 2016, **7**, 2639.
14 Z. Y. Lu, L. Qian, Y. Tian, Y. P. Li, X. M. Sun and X. Duan, *Chem. Commun.*, 2016, **52**, 908.
15 Z. Q. Liu, N. Li, H. Y. Zhao, Y. Zhang, Y. H. Huang, Z. Y. Yin and Y. P. Du, *Chem. Sci.*, 2017, **8**, 3211.
16 J. F. Xie, X. D. Zhang, H. Zhang, J. J. Zhang, S. Li, R. X. Wang, B. C. Pan and Y. Xie, *Adv. Mater.*, 2017, **29**, 1604764.
17 K. Fominykh, G. C. Tok, P. Zeller, H. Hajiyani, T. Miller, M. Doblinger, R. Pentcheva, T. Bein and D. Fattakhova-Rohlfing, *Adv. Funct. Mater.*, 2017, **27**, 1605121.
18 F. Malara, S. Carallo, E. Rotunno, L. Lazzarini, E. Piperopoulos, C. Milone and A. Naldoni, *ACS Catal.*, 2017, **7**, 4786.
19 M. Gong, Y. G. Li, H. L. Wang, Y. Y. Liang, J. Z. Wu, J. G. Zhou, J. Wang, T. Regier, F. Wei and H. J. Dai, *J. Am. Chem. Soc.*, 2013, **135**, 8452.
20 L. Trotochaud, S. L. Young, J. K. Ranney and S. W. Boettcher, *J. Am. Chem. Soc.*, 2014, **136**, 6744.
21 J. W. D. Ng, M. Garcia-Melchor, M. Bajdich, P. Chakthranont, C. Kirk, A. Vojvodic and T. F. Jaramillo, *Nat. Energy*, 2016, **1**, 1.
22 M. B. Stevens, C. D. M. Trang, L. J. Enman, J. Deng and S. W. Boettcher, *J. Am. Chem. Soc.*, 2017, **139**, 11361.
23 M. A. Lukowski, A. S. Daniel, F. Meng, A. Forticaux, L. S. Li and S. Jin, *J. Am. Chem. Soc.*, 2013, **135**, 10274.
24 M. Asadi, K. Kim, C. Liu, A. V. Addepalli, P. Abbasi, P. Yasaei, P. Phillips, A. Behranginia, J. M. Cerrato, R. Haasch, P. Zapol, B. Kumar, R. F. Klie, J. Abiade, L. A. Curtiss and A. Salehi-Khojin, *Science*, 2016, **353**, 467.
25 S. Gao, Y. Lin, X. C. Jiao, Y. F. Sun, Q. Q. Luo, W. H. Zhang, D. Q. Li, J. L. Yang and Y. Xie, *Nature*, 2016, **529**, 68.
26 X. Peng, Y. Q. Guo, Q. Yin, J. C. Wu, J. Y. Zhao, C. M. Wang, S. Tao, W. S. Chu, C. Z. Wu and Y. Xie, *J. Am. Chem. Soc.*, 2017, **139**, 5242.

 This journal is © The Royal Society of Chemistry 2018

Published on 12 February 2018. Downloaded by University of Wisconsin - Madison on 21/03/2018 19:01:49.

27 C. L. Tan, X. H. Cao, X. J. Wu, Q. Y. He, J. Yang, X. Zhang, J. Z. Chen, W. Zhao, S. K. Han, G. H. Nam, M. Sindoro and H. Zhang, *Chem. Rev.*, 2017, **117**, 6225.
28 Y. H. Dou, L. Zhang, X. Xu, Z. Q. Sun, T. Liao and S. X. Dou, *Chem. Soc. Rev.*, 2017, **46**, 7338.
29 Z. M. Hu, X. Xiao, H. Y. Jin, T. Q. Li, M. Chen, Z. Liang, Z. F. Guo, J. Li, J. Wan, L. Huang, Y. R. Zhang, G. Feng and J. Zhou, *Nat. Commun.*, 2017, **8**, 1.
30 F. Wang, J. H. Seo, G. F. Luo, M. B. Starr, Z. D. Li, D. L. Geng, X. Yin, S. Y. Wang, D. G. Fraser, D. Morgan, Z. Q. Ma and X. D. Wang, *Nat. Commun.*, 2016, **7**, 1.
31 F. Wang, Y. H. Yu, X. Yin, P. Tian and X. D. Wang, *J. Mater. Chem. A*, 2017, **5**, 9060.
32 X. Yin, Y. Q. Shi, Y. B. Wei, Y. Joo, P. Gopalan, I. Szlufarska and X. D. Wang, *Langmuir*, 2017, **33**, 7708.
33 L. H. Wu, Q. Li, C. H. Wu, H. Y. Zhu, A. Mendoza-Garcia, B. Shen, J. H. Guo and S. H. Sun, *J. Am. Chem. Soc.*, 2015, **137**, 7071.
34 J. X. Feng, H. Xu, Y. T. Dong, S. H. Ye, Y. X. Tong and G. R. Li, *Angew. Chem., Int. Ed.*, 2016, **55**, 3694.
35 X. F. Lu, L. F. Gu, J. W. Wang, J. X. Wu, P. Q. Liao and G. R. Li, *Adv. Mater.*, 2017, **29**, 1604437.
36 F. Song and X. L. Hu, *Nat. Commun.*, 2014, **5**, 1.
37 K. L. Nardi, N. Y. Yang, C. F. Dickens, A. L. Strickler and S. F. Bent, *Adv. Energy Mater.*, 2015, **5**, 1500412.
38 A. C. Pebley, E. Decolvenaere, T. M. Pollocka and M. J. Gordon, *Nanoscale*, 2017, **9**, 15070.